ORNL/TM--9210

DE85 001732

Fusion Energy Division

ELECTRON BOUNCE RESONANCE HEATING IN A BUMPY CYLINDER

G. L. Chen

DISCLAIMER

This report was prepared as an account of work sponsored by an agency of the United States Government. Neither the United States Government nor any agency thereof, nor any of their employees, makes any warranty, express or implied, or assumes any legal liability or responsibility for the accuracy, completeness, or usefulness of any information, apparatus, product, or process disclosed, or represents that its use would not infringe privately owned rights. Reference herein to any specific commercial product, process, or service by trade name, trademark, manufacturer, or otherwise does not necessarily constitute or imply its endorsement, recommendation, or favoring by the United States Government or any agency thereof. The views and opinions of authors expressed herein do not necessarily state or reflect those of the United States Government or any agency thereof.

Date Published - October 1984

Prepared by the
OAK RIDGE NATIONAL LABORATORY
Oak Ridge, Tennessee 37831
operated by
MARTIN MARIETTA ENERGY SYSTEMS, INC.
for the
U.S. DEPARTMENT OF ENERGY
under Contract No. DE-AC05-84OR21400

MASTER

DISTRIBUTION OF THIS DOCUMENT IS UNLIMITED

CONTENTS

ABSTRACT

In bumpy cylinder geometry, the electrons are classified into trapped and passing particles. The interaction between a wave near the electron bounce frequency and the electrons is studied both numerically and analytically for the appropriate parameters of ELMO Bumpy Torus-Scale (EBT-S). It is shown that coupling of the waves to the electron bounce motion parallel to the magnetic field can lead to heating of those electrons near the passing/trapped boundary in velocity space. The stochastic threshold condition is $eE_0k_0/m\omega_b^2 \simeq 0.1$. For this mechanism, it is found that the wave energy density required to induce stochastic heating in EBT by rf [in the frequency range of ion cyclotron resonance heating (ICRH)] is about an order of magnitude more than that estimated on the basis of cold plasma wave theory. It is hypothesized that this discrepancy would disappear when the thermal correction to the wave propagation and the effects of collisions and toroidicity are included. We also suggest that the bounce resonance can enhance the electron cyclotron resonance heating (ECRH) efficiency in an EBT-like heating scheme.

I. INTRODUCTION

Recent work[1] on charged particle heating by wave particle bounce resonance processes in tokamaks and mirrors has assumed a quadratic magnetic well ($B \propto 1 + z^2/L^2$) or uniform magnetic field. Under these conditions, the required threshold wave amplitude for stochastic electron motion is $eE_0k_0/m\omega_b^2 \geq 1$. In a bumpy magnetic system such as Elmo Bumpy Torus (EBT), however, the magnetic field variation along a field line is more accurately modeled by $B = B_0[1 - \epsilon \cos(k_0 z)]$. The electrons can then be cataloged into mirror-trapped and passing electrons. Passing electrons circulate completely around the torus. A transition between the two groups of electrons occurs near the separatrix (the location of the maximum field). At a very weak wave perturbation (i.e., $eE_0k_0/m\omega_b^2 \leq 0.1$), the electrons' motion near the separatrix becomes chaotic. The electrons are heated by this tiny disturbance. Two effects, collisions[1] and toroidicity,[2] that could increase the stochasticity and reduce the threshold E_0 are not considered here.

The heating theory presented in this paper has been motivated by recent experimental observations of hot electron ring heating during which ion cyclotron range of frequency (ICRF) wave heating on EBT-S.[3] The hot electron ring is generated by electron cyclotron resonance heating (ECRH). The ring temperature is about 500 KeV without the ICRF heating. With the application of ion cyclotron resonance heating (ICRH), the ring stored energy ($nT_{ring} \times V_{ring}$) approximately doubles at a power level of 15 kW.[3] It will be shown in Sec. III that the stochastic heating process presented here may not explain the ring energy increases based upon imposed cold plasma fast magnetosonic wave fields. Other waves having a large parallel electric field are

required to induce substantial stochastic heating. It has been shown that the fast wave by itself cannot directly heat the ions in EBT-Scale (EBT-S). Using hot-plasma theory and Monte-Carlo calculations, ion-Bernstein waves have been postulated to play a role in ICRH on EBT.[4] The presence of ion-Bernstein waves in the EBT experiment may induce a much stronger stochastic heating of electrons than would the fast wave.

The equation of motion that we study in this paper was first used to study the stochastic instability of magnetic trapped particles by Zaslavskii and Filonenko[5] in 1968. Escande[6] has applied the renormalization method on the same equation to obtain the stochasticity threshold condition. In Sec. II, we derive a single-particle motion model from the Hamiltonian. Results of the calculation and the application to rf heating in EBT are presented in Sec. III. The conclusions and a discussion are found in Sec. IV.

II. EQUATION OF MOTION

A. Basic equation

We consider an idealized magnetic field model for EBT as shown in Fig. 1. Here, we assume an infinitely long axisymmetric and periodic bumpy cylinder. This field is given by

$$\overline{B} = B_r\hat{r} + B_z\hat{z} \quad , \tag{1}$$

where $\hat{r}$ and $\hat{z}$ are unit vectors in the radial and axial direction, respectively, and

$$B_r = -B_0\epsilon I_1(k_0 r)\sin(k_0 z) \quad , \tag{2a}$$

$$B_z = B_0[1 - \epsilon I_0(k_0 r)\cos(k_0 z)] \quad . \tag{2b}$$

Here $k_0 = \pi/L$, L is half of one mirror cell length, I_0 and I_1 are Bessel functions, and ϵ is related to the mirror ratio M by $\epsilon = (M - 1)/(M + 1)$. We will consider ϵ and $k_0 r$ as the small parameters in the following discussion; that is, we let $I_1(k_0 r) = 0$ and $I_0(k_0 r) = 1$ in Eq. (2).

The vector potential corresponding to this model is then

$$\overline{A} = A_\theta\hat{\theta} \quad , \tag{3a}$$

where

$$\hat{\theta} = \hat{z} \times \hat{r} \quad ,$$

$$A_\theta \simeq B_0(r - r\epsilon \cos k_0 z) \quad . \tag{3b}$$

In cylindrical coordinates, the Hamiltonian can be rewritten as

$$H_0 = \frac{1}{2}\left[P_r^2 + P_z^2 + \left(P_\theta - \frac{e}{mc} A_\theta\right)^2\right] \quad . \tag{4}$$

Substituting Eq. (3b) into Eq. (4) and keeping only terms of order ϵ, we obtain

$$H = H_0 - \mu B = \frac{1}{2} P_z^2 - \epsilon\mu B_0 \cos k_0 z \quad . \tag{5}$$

For the adiabatic particles ($\mu B_0 \simeq$ constant), the constant of motion is H. Adding the wave perturbation to Eq. (5), the energy of the particle becomes a function of time and is

$$H = \frac{1}{2} P_z^2 - \epsilon\mu B_0 \cos k_0 z - \frac{eE_0}{k_\parallel} \cos\left(k_\parallel z - \omega t\right) \quad , \tag{6}$$

where E_0 is the parallel component of electric field strength of the rf wave and $k_\parallel$ and ω are the corresponding wave vector and frequency, respectively. Figure 2 shows a contour plot of unperturbed $H(P_z, z)$ [Eq. (5)]. The gross structure of this picture is not changed very much by a small amplitude wave field. However, in the next section, we will show that the motion of those particles near the vicinity of the separatrix (x points of Fig. 2) becomes stochastic.

The equation of motion from Eq. (6) can be written as

$$\frac{dv_\parallel}{dt} + \epsilon\mu B_0 k_0 \sin k_0 z + eE_0 \sin\left(k_\parallel z - \omega t\right) = 0 \quad , \tag{7a}$$

where $v_{\parallel} = \dot{z} = dz/dt$. Here, we let $m_e = 1$. By defining $\omega_b^2 = \epsilon\mu B_0 k_0^2$, $x = k_0 z$, $k = k_{\parallel}/k_0$, $\nu = \omega/\omega_b$, and $T = \omega_b t$, we can obtain the dimensionless equation of motion:

$$\frac{d^2x}{dT^2} + \sin x + \alpha \sin(kx - \nu T) = 0 \quad , \tag{7b}$$

where $\alpha = eE_0 k_0/\omega_b^2$ and $dx/dT = V_{\parallel} = k_0 v/\omega_b$. For small x, $\sin x \simeq x$, Eq. (7b) can be reduced to $d^2x/dT^2 + x + \alpha \sin(kx - \nu T) = 0$. This equation has been discussed in Ref. 1. It is interesting to point out that Eq. (7b) implies a particle interaction with a standing wave and a traveling wave if $\alpha \ll 1$. For our purpose, we only discuss the situation with small α and integer ν, $\nu = 1, 2, 3, \ldots$.

B. Unperturbed solution

When $\alpha = 0$, the solution of Eq. (7b) is well known from the theory of the free oscillations of a pendulum.[5] For trapped particles,

$$I = \frac{1}{2p} \oint \dot{x}\, dx$$

$$= \frac{8}{\pi} \left[E(q) - (1 - q^2)K(q)\right] \quad , \tag{8a}$$

$$\Omega = \frac{d\theta}{dT} = \frac{\pi\omega_b}{2K(q)} \quad , \tag{8b}$$

$$\dot{x} = 2qcn(T) \quad , \tag{8c}$$

and for untrapped particles,

$$I = \frac{1}{2\pi} \int_0^{2\pi} \dot{x}\, dx$$

$$= \frac{8}{\pi} q\text{-}(\frac{1}{q}) \quad , \tag{9a}$$

$$\Omega = \frac{\pi q \omega_b}{K(1/q)} \quad , \tag{9b}$$

$$\dot{x} = 2qdn(T) \quad , \tag{9c}$$

where $q^2 = 1/2(1 + H)$, E and K are the complete elliptic integrals, and cn and dn are Jacobian elliptic functions. The parameter q is related to the cosine of the pitch angle at the midplane, $\zeta_m = V_{||}/V|_{x=0}$, by

$$q = \frac{\zeta_m}{\sqrt{(M - 1)(1 - \zeta_m^2)}} \, . \tag{10a}$$

and related to the energy, $E_{||}$ and $E_{\perp}$, by

$$q^2 = \frac{E_{||}}{(M - 1)E_{\perp}} \, . \tag{10b}$$

In the following sections, it will be useful to note that the separatrix ($H \to 1$, $q \to 1$, and $\Omega \to 0$) of particle motion in velocity space occurs near $V_{||0} \equiv V_{||}|_{x=0} = 2$.[5] This is most easily seen in terms of the pendulum analog by recognizing that the maximum potential energy difference is 2 in the present notation whereas the kinetic energy is $1/2V_{||0}^2$ at x=0 (the point of minimum potential energy).

In order to see the difference between our model and the quadratic magnetic field model, we compare the unperturbed solutions in both cases. A plot of Ω versus q, Eqs. (8b) and (9b), for different ω_b is shown in Fig. 3(a). If the quadratic magnetic field is used, Eqs. (8b) and (9b) can be written simply as $\Omega = \omega_b$ for all q. Then, the curves in Fig. 3(a) become straight horizontal lines (constant). However, we can see that here the curves merge together and approach zero at the point $q = 1$ (the separatrix). This implies much greater resonance overlap at the separatrix ($q = 1$), if a perturbation is applied. Since resonance overlap causes stochasticity,[7] the required stochastic threshold wave amplitude is found to be a factor of 10 less for the sinusoidal well than in previous work using a parabolic well.[1] In the next section we will see that only $\alpha \simeq 0.1$ is needed to produce stochasticity compared to $\alpha \geq 1$ for the parabolic well. Figure 3(a) shows that the resonance frequency decreases as the cosine of the pitch angle increases for trapped particles and then again increases for increasing q or ζ_m for passing particles. Figure 3(b) is a contour plot of Ω versus the energy, $E_{\parallel}$ and $E_{\perp}$. This plot tells us the relationship between particle energy, pitch angle, and bounce frequency. For example, a 30-MHz ICRH wave is resonant with those electrons that have $T_{e\perp} = 3$ keV when $V_{\parallel 0} = 0$ and with those electrons that have higher energy at or near $q = 1$.

III. NUMERICAL RESULTS AND APPLICATION TO HEATING

We use the codes, LSODA and LSODAR,[8] to solve Eq. (7b). Some typical particle trajectories are shown in Fig. 4. For deeply trapped particles ($V_{\|0} \ll 2$) or strongly passing particles, the motion is a periodic oscillation as expected. However, those particles near the separatrix ($V_{\|0} \simeq 2$) show transitional motion — being detrapped or retrapped by the wave.

In order to reduce the three-dimensional character of $\dot{x}$, x, and T, we plot the surface of section,[1] defined by $x = 0$ for trapped particles or $x = n\pi$ for passing particles. The particle trajectory is then a series of dots on the $\dot{x}$-νT plane where LSODAR is used to find the root of $x(\dot{x},T) = 0$. In Figs. 5–7, we show a sequence of surface of section plots for ν from 1.0 to 4.0 with $\alpha = 0.05$ to 0.2. A stochastic motion strip is always present near $V_{\|0} = 2$ (the separatrix). For this small α, no random motion occurs if one assumes a quadratic magnetic field. The width of random motion region increases as α increases. The islands or smooth curves correspond to the existence of an adiabatic invariant of motion. The number of islands is determined by the integer $\nu = \omega/\omega_b$. As α is increased, these islands expand and overlap together; then, the particle motion becomes stochastic over all the trapped region ($V_{\|0} \leq 2$). From Figs. 5–7, we also can see that the external waves not only induce the stochasticity near the separatrix but also push nonstochastic low $V_{\|}/V$ particles to a high $V_{\|}/V$ over part of their trajectory. This is an important result and will be discussed later.

Figure 8 shows the upper bound (untrapped region) and lower bound (trapped region) on the velocity of the stochastic motion region for $\alpha = 0.1$. The solid line is obtained from our numerical calculations and the dashed line is reproduced from renormalization theory by Escande.[6] The two results are in reasonable agreement. A maximum that implies strongest resonance effects appears near $\nu = 2$ because the particles get longer kicks through the waves. The strength of the kick is the same for all ν. For a particular wave, α and ν are the only two variables that determine the character of the surface of sections. The above results would apply to any plasma that has magnetic ripple.

We now estimate the heating produced by the stochastic motion induced by the parallel electric field. The simplest way to study heating is to compute $\langle V_{\|}^2 \rangle$ from the trajectory calculation, where $\langle \ldots \rangle$ means ensemble average. This quantity is proportional to the parallel energy and diffusion coefficient. To do this average, we use 200 particles with random initial velocity within $|V_{\|0}| \leq 4$ and initial position inside $0 \leq x \leq 2\pi$. The typical time evolution of this quantity, which is normalized to $\langle V_{\|}^2(T = 0) \rangle$, is shown in Fig. 9. The rapid increase in $\langle V_{\|}^2 \rangle$ of particles is observed within a time of $T = 2 \times 10^4$. This is followed by a slower increase, which implies the heating processes are saturated, because the particles have spread out to fill the whole stochastic region of velocity space. By remembering that we define $T \equiv \omega_b t$, $T = 2 \times 10^4$ is equivalent to the time period of 2×10^4 particle bounces. In Fig. 9 we have taken $\nu = 1$ and $\alpha = 0.1$. For the case illustrated in Fig. 9, $\langle V_{\|}^2 \rangle$ increased by a factor of 5 during the ion cyclotron heating. The diffusion rate can obtained from the linear part of curve.

To estimate the energy increases, we assume that we have n electrons in this group. The total energy of those particles before the heating is

$$E_B = \frac{1}{2} nm_e(\langle v_{\parallel}^2\rangle_B + \langle v_{\perp}^2\rangle_B) \; ; \tag{11}$$

after the heating it is

$$E_A = \frac{1}{2} nm_e(\langle v_{\parallel}^2\rangle_A + \langle v_{\perp}^2\rangle_A) = \frac{1}{2} nm_e(5\langle v_{\parallel}^2\rangle_B + \langle v_{\perp}^2\rangle_A) \; , \tag{12}$$

where the indexes A and B represent after and before heating, respectively. We have assumed that these electrons have μB_o constant. Hence, we expect that $\langle v_{\perp}^2\rangle_B \simeq \langle v_{\perp}^2\rangle_A$. Furthermore, we know that for the resonance particles

$$v_{\parallel B} \sim \frac{\omega}{k_{\parallel}} \sim \frac{\nu\omega_b}{k_{\parallel}} \; , \tag{13}$$

and, from the definition of ω_b, we have

$$v_{\perp B} \sim \frac{2\omega_b}{\sqrt{\epsilon} k_{\parallel}} = \frac{3\omega}{k_{\parallel}} \; . \tag{14}$$

Hence, $V_{\parallel B} \sim \nu/3V_{\perp B}$ and, therefore, $(E_A/E_B) \sim 2$, if we assume $\nu = 1$ and $\epsilon = 0.5$.

From this example, we have shown that the electrons could be heated by rf wave, if the rf wave field is strong enough. We summarize the results of stochastic heating in Tables 2 and 3. Table 2 gives E_0 for different α and ν. The third column shows the initial temperature of the resonant electron. In Table 3, we list the increase of $\langle V_{\parallel}^2 \rangle$ for different ν with $\alpha = 0.1$. From both tables, we observe that a group of 2.399-keV ($Te_{\perp}$) electrons can be heated by 30-MHz ion cyclotron waves to about twice their initial energy if the waves have an electric field strength of 12.88 V/cm. The corresponding electron trajectory is shown in Fig. 6(a). However, for 150-eV electrons, we need an electric field of only 0.4 V/cm [see Table 3 and Fig. 5(d)]. If we include the effects of collisions and toroidicity, the threshold electric field could be lowered.

The increase of the cosine of the pitch angle is another effect of an rf wave field. In EBT the electrons are basically heated by electron cyclotron resonance heating (ECRH), from the fundamental resonance near $L = \pm 10$ cm and the second harmonic resonance near the midplane. Not all of the electrons can be heated by fundamental resonance unless they can cross the heating zone. We list in Table 4 locations of the ring boundary, ECRH resonance, and separatrix in velocity space for EBT-S. From orbit plots [for example Fig. 6(a)], we can see that the lower $V_{\parallel}$ electrons are pushed up to the fundamental resonance zone ($V_{\parallel} = 1.414$), at which point they could be heated by ECRH. Hence, the electron bounce resonance with ion cyclotron waves could increase the ECRH efficiency.

IV. DISCUSSION AND CONCLUSIONS

We have demonstrated that the electrons are heated in the direction along the magnetic field due to bounce resonance with waves if the electric field parameter of the wave satisfies $\alpha \simeq 0.1$. The stochastic threshold criterion α is a factor of 10 less than previous works[1] if we include the the transition motion between passing and trapped particles. The transition motion has not been considered previously.

We conclude that our theory predicts stochastic heating of transitional electrons with low $T_{\perp e}$. It also predicts increases in $V_{\parallel}/V$. Hence, in EBT, if the rf wave field strength can satisfy the threshold condition ($\alpha \simeq 0.1$), the bounce resonance may be considered as a catalyst that pushes electrons to energies and pitch angles where the ECRH becomes important. These effects essentially feed particles into the part of velocity space where second harmonic electron cyclotron absorption is strong. Experimental identification of this population of feed electrons has not been made although large increases in the hot electron ring energy have been measured.[4] This hypothesis will have to remain speculative in the absence of a measurement of changes in feed electrons.

In most tokamaks and reactors, the field strength required to induce stochastic effects is easily satisfied. We do not have experimental results to determine if our E_0 is reasonable in EBT-S. However, the cold plasma theory[9] for fast ion cyclotron waves predicts E_0 is about 0.1 V/cm for 10 kW of wave power. This field amplitude is below the threshold for stochastic heating predicted above. The implication is that the fast wave cannot induce stochasticity of the type described in this paper. Recently, Monte-Carlo results[3] have

shown that the fast wave by itself cannot heat the ions. An electrostatic wave, the ion-Bernstein wave, may instead be responsible for the observed ion heating.[4] The ion-Bernstein waves could supply the larger parallel electric fields needed to induce stochasticity in electrons. The detailed structure of ICRH wave fields in an EBT configuration is currently under investigation.[10]

ACKNOWLEDGMENTS

This work was supported by the Office of Fusion Energy, U.S. Department of Energy, under Contract No. DE-AC05-84OR21400 with Martin Marietta Energy Systems, Inc. The author wishes to thank Drs. D. B. Batchelor and T. L. Owens for useful discussions and for helpful critical readings of this paper.

FIGURE CAPTIONS

FIG. 1. EBT magnetic field configuration.

FIG. 2. Unperturbed particle orbits in phase space.

FIG. 3. (a) A plot of Ω vs q. (b) The contour plot of Ω vs energy, $E_{\parallel}$ and $E_{\perp}$. No passing region is shown. The first contour is 11.18 MHz and the increment is 2.36 MHz. We use EBT-S parameters here.

FIG. 4. The typical plot of particle trajectories represented by both x vs time (dashed line) and $V_{\parallel}$ vs time (solid line).

FIG. 5. A plot of surface of section for $\alpha = 0.05$ (low field) with (a) $\nu = 1$, (b) $\nu = 2$, (c) $\nu = 3$, and (d) $\nu = 4$

FIG. 6. A plot of surface of section for $\alpha = 0.2$ with (a) $\nu = 1$, (b) $\nu = 2$, (c) $\nu = 3$, and (d) $\nu = 4$

FIG. 7. A plot of surface of section for $\alpha = 0.2$ (high field) with (a) $\nu = 1$, (b) $\nu = 2$, (c) $\nu = 3$, and (d) $\nu = 4$

FIG. 8. Stochastic boundary layer.

FIG. 9. The typical time evolution of $\langle V_{\parallel}^2 \rangle$.

REFERENCES

[1]C. F. F. Karney, Phys. Fluids 21, 1584 (1978); J. Y. Hsu, Phys. Fluids 25, 159 (1982); K. C. Shaing and J. D. Callen, University of Wisconsin Report UWFDM-463, Madison, Wisconsin.

[2]L. E. Deleanu, L. W. Owen, and G. L. Chen, Bull. Am. Phys. Soc. 27, 1087 (1982).

[3]T. L. Owens, J. H. Mullen, F. W. Baity, W. A. Davis, O. C. Eldridge, and D. L. Hillis, Nucl. Fusion 23, 49 (1983).

[4]"Ion heating in the range of high ion cyclotron harmonics on EBT", T. L. Owens, F. W. Baity, and W. A. Davis, (submitted to Nucl. Fusion), P. L. Colestock and P. J. Kashuba, Nucl. Fusion 23, 763 (1983).

[5]G. M. Zaslavskii and N. N. Filonenko, Sov. Phys. JETP 25, 851 (1968)

[6]D. F. Escande, Long Time Prediction in Dynamics (John Wiley and Sons, New York, 1982), p. 149.

[7]G. R. Smith, Phys. Rev. Lett. 38, 970 (1977); B. V. Chivikov, Phys. Rev. 52, 263 (1979)

[8]L. R. Petzold and A. C. Hindmarsh, "Livermore Solver for Ordinary Differential Equations With Automatic Method Switching for Stiff and

Nonstiff Problems," Lawrence Livermore National Laboratory, Livermore, California.

[9]D. A. Bower et al., McDonnell Douglas Astronautics Company, St. Louis Division, Report MDC E2248 (April 1980)

[10]D. B. Batchelor, C. W. Nestor, and H. Weitzner, Bull. Am. Phys. Soc. 28, 1041 (1983).

Table 1. EBT-S parameters (at ring)

Half mirror cell length, L (cm)	20
Mirror ratio, M	3
Magnetic field origin, B_0 (T)	1.0
ICRH wave frequency, f (MHz)	15~50
Collision frequency for $T_e \sim 0.6$ keV, ν_e (Hz)	10^4
Density (cm^{-3})	10^{12}
ECRH wave frequency, f_{ECRH} (GHz)	28
Position of ECRH fundamental resonance, L_s (cm)	~10

Table 2. The corresponding E_0 for different ν and α (with EBT-S parameters)

ν	ω_b (Mhz)	$T_{e\perp}$ (eV)	E_0(V/cm) $\alpha = 0.05$	$\alpha = 0.1$	$\alpha = 0.2$
1	$2\pi \times 30.0$	2399	6.44	12.88	25.76
2	$2\pi \times 15.0$	599	1.60	3.20	6.40
3	$2\pi \times 10.0$	266	0.72	1.43	2.83
4	$2\pi \times 7.5$	150	0.40	0.81	1.61

Table 3. $\langle V_{\parallel}^2 \rangle / \langle V_{\parallel}^2 (T = 0) \rangle$ and E_A/E_B for different ν with $\alpha = 0.1$

ν	$\langle V_{\parallel}^2 \rangle / \langle V_{\parallel}^2 (T=0) \rangle$	E_A/E_B
1.0	5.0	2.0
1.3	6.3	2.6
1.5	7.5	3.2
2.0	12.0	5.4

Table 4. Some interesting locations in velocity space (M = 3)

	$V_{\parallel}$	ζ_m	$q(\zeta_m)$
Second resonance (midplane)	0	0	0
Fundamental resonance	1.414	0.707	0.707
Separatrix	2.000	0.816	1.000

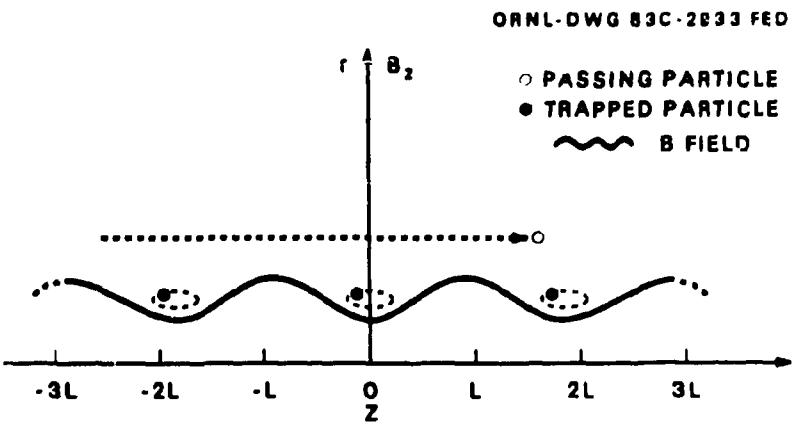
ORNL-DWG 83C-2833 FED
r
B_z
PASSING PARTICLE
TRAPPED PARTICLE
B FIELD
-3L
-2L
-L
0
L
2L
3L
Z

FIG. 1.

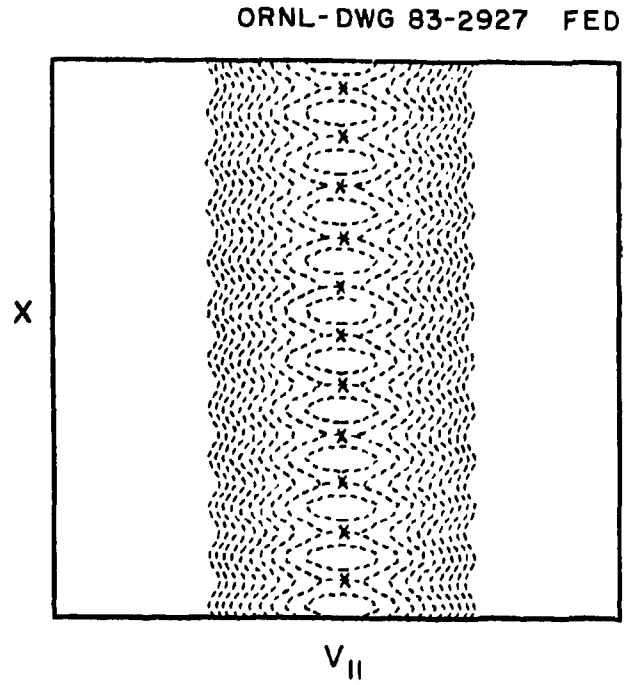

FIG. 2.

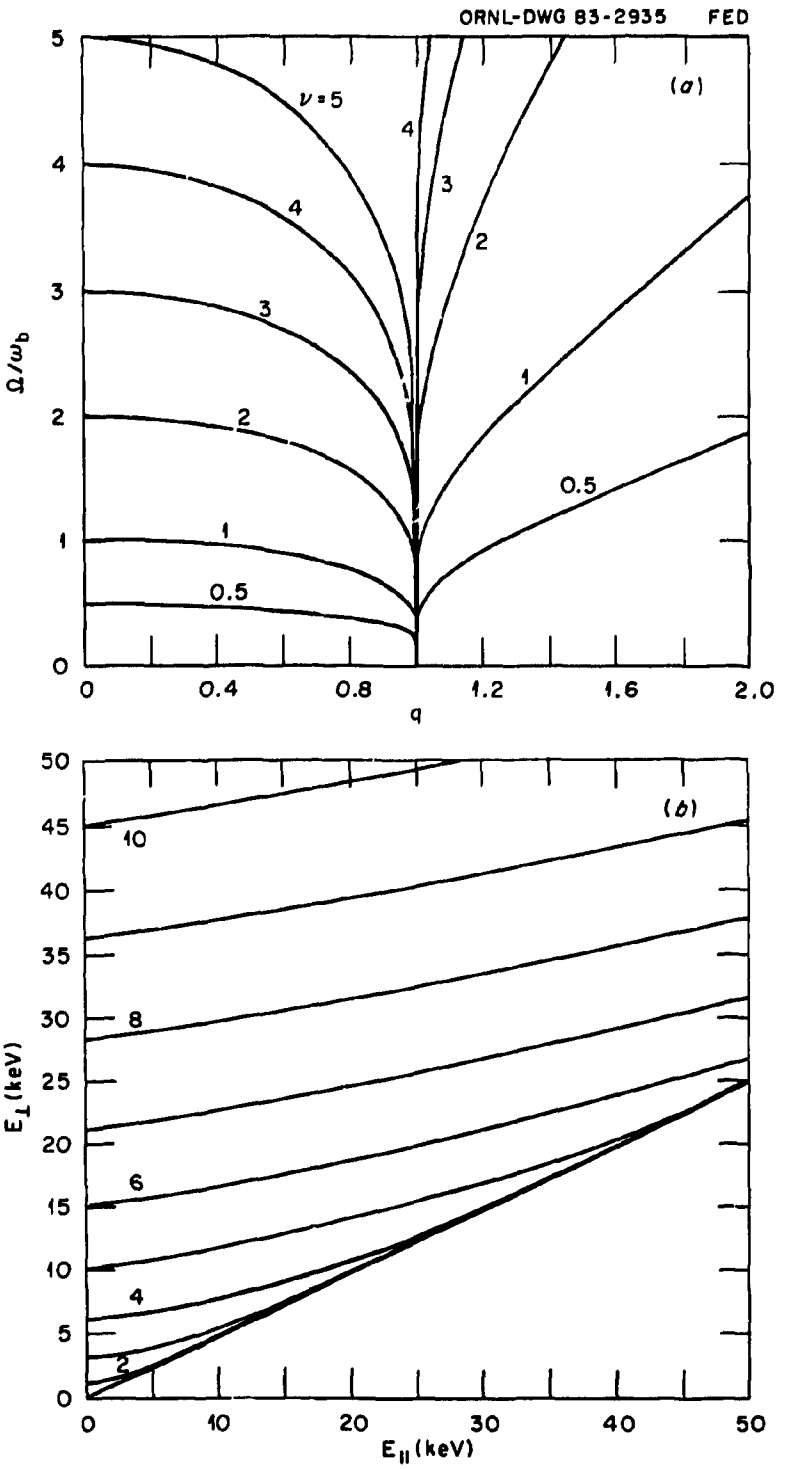

FIG. 3.

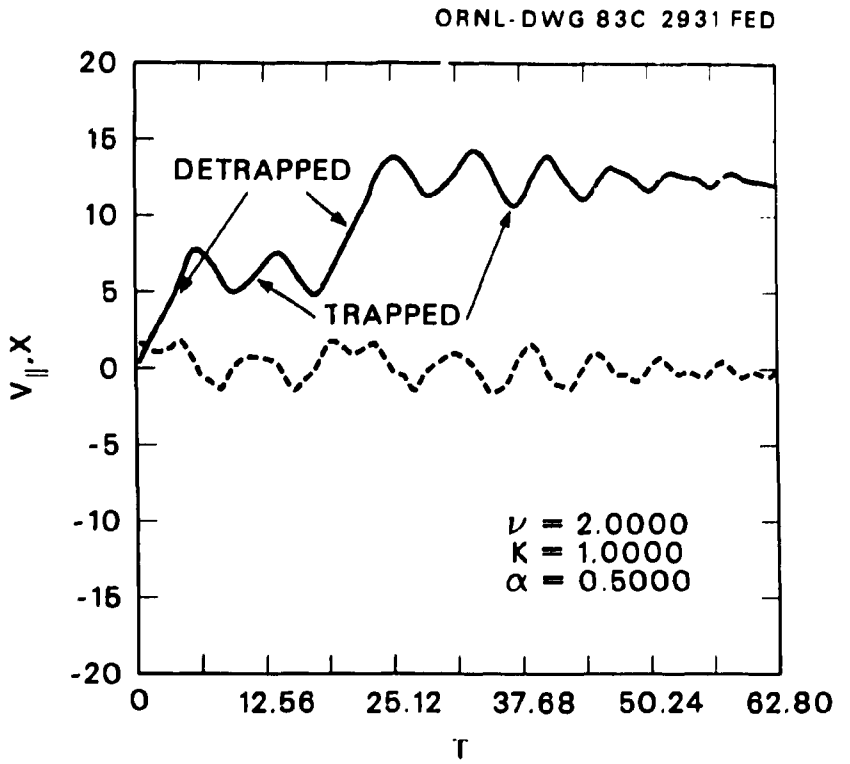
ORNL-DWG 83C 2931 FED
20
15
10
5
0
-5
-10
-15
-20
0
12.56
25.12
37.68
50.24
62.80
τ
$v_{\parallel}$ x
DETRAPPED
TRAPPED
ν = 2.0000
K = 1.0000
α = 0.5000

FIG. 4.

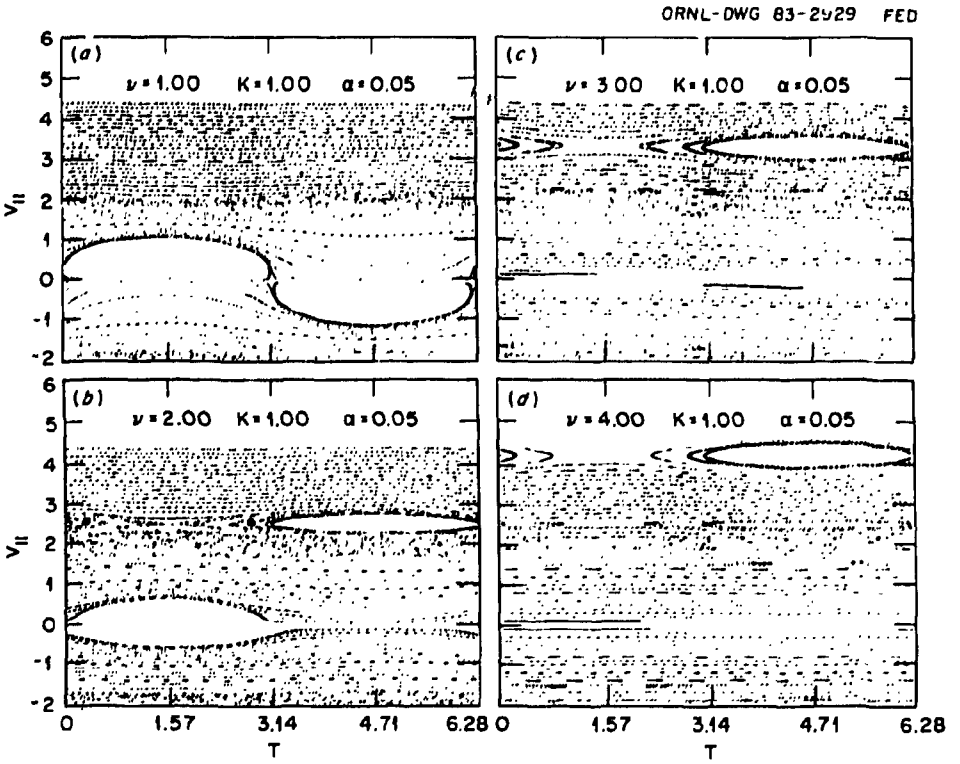
ORNL-DWG 83-2929 FED
(a)
ν = 1.00 K = 1.00 α = 0.05
(c)
ν = 3.00 K = 1.00 α = 0.05
(b)
ν = 2.00 K = 1.00 α = 0.05
(d)
ν = 4.00 K = 1.00 α = 0.05
$v_{||}$
T
0
1.57
3.14
4.71
6.28

FIG. 5.

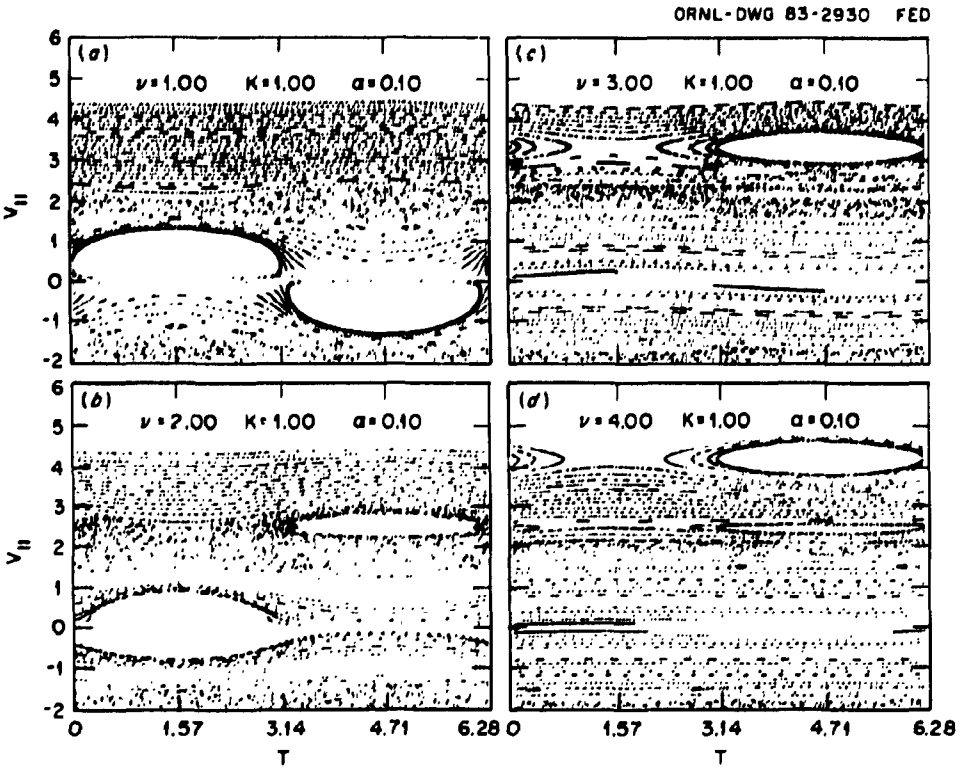
ORNL-DWG 83-2930 FED
(a)
ν = 1.00 K = 1.00 α = 0.10
(c)
ν = 3.00 K = 1.00 α = 0.10
(b)
ν = 2.00 K = 1.00 α = 0.10
(d)
ν = 4.00 K = 1.00 α = 0.10
v∥
T
0
1.57
3.14
4.71
6.28

FIG. 6.

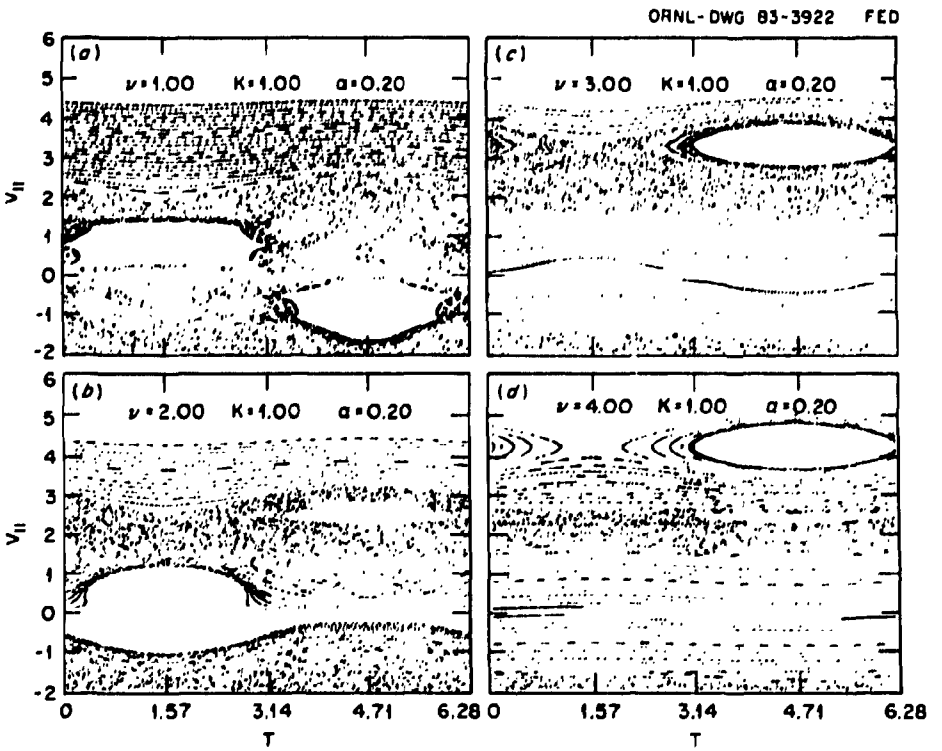
ORNL-DWG 83-3922 FED
(a)
ν=1.00 K=1.00 α=0.20
(c)
ν=3.00 K=1.00 α=0.20
(b)
ν=2.00 K=1.00 α=0.20
(d)
ν=4.00 K=1.00 α=0.20
v∥
T
0
1.57
3.14
4.71
6.28

FIG. 7.

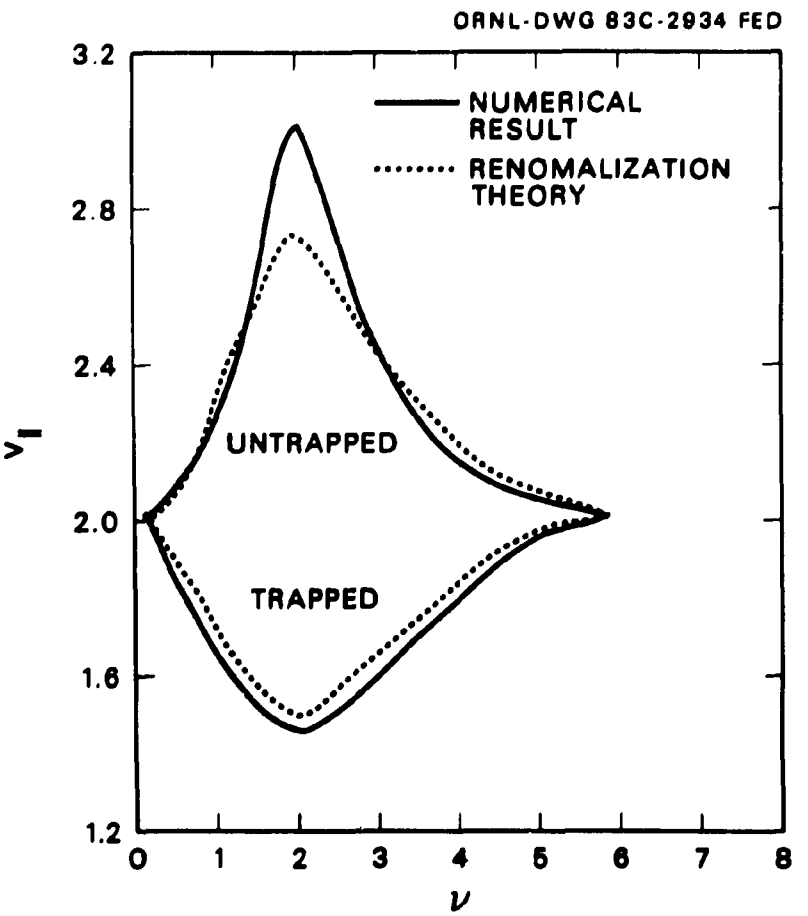
ORNL-DWG 83C-2934 FED
NUMERICAL RESULT
RENOMALIZATION THEORY
UNTRAPPED
TRAPPED
3.2
2.8
2.4
2.0
1.6
1.2
0
1
2
3
4
5
6
7
8
ν
ν

FIG. 8.

ORNL/TM-9210
Dist. Category UC-20

INTERNAL DISTRIBUTION

1. B. A. Carreras
2-6. G. L. Chen
7. S. Hiroe
8. T. L. Owens
9. J. Sheffield
10. D. A. Spong
11-12. Laboratory Records Dept.
13. Laboratory Records, ORNL-RC
14. Document Reference Section
15. Central Research Library
16. Fusion Energy Division Library
17. Fusion Energy Division Publications Office
18. ORNL Patent Office

EXTERNAL DISTRIBUTION

19. Office of the Assistant Manager for Energy Research and Development, Department of Energy, Oak Ridge Operations, Box E, Oak Ridge, TN 37830
20. J. D. Callen, Department of Nuclear Engineering, University of Wisconsin, Madison, WI 53706
21. R. W. Conn, Department of Chemical, Nuclear, and Thermal Engineering, University of California, Los Angeles, CA 90024
22. S. O. Dean, Director, Fusion Energy Development, Science Applications, Inc., 2 Professional Drive, Gaithersburg, MD 20760
23. H. K. Forsen, Bechtel Group, Inc., Research Engineering, P.O. Box 3965, San Francisco, CA 94105
24. R. W. Gould, Department of Applied Physics, California Institute of Technology, Pasadena, CA 91125
25. D. G. McAlees, Exxon Nuclear Company, Inc., 777 106th Avenue, NE, Bellevue, WA 98009
26. P. J. Reardon, Princeton Plasma Physics Laboratory, P.O. Box 451, Princeton, NJ 08544
27. W. M. Stacey, Jr., School of Nuclear Engineering, Georgia Institute of Technology, Atlanta, GA 30332
28. G. A. Eliseev, I. V. Kurchatov Institute of Atomic Energy, P.O. Box 3402, 123182 Moscow, U.S.S.R.
29. V. A. Glukhikh, Scientific-Research Institute of Electro-Physical Apparatus, 188631 Leningrad, U.S.S.R.
30. I. Spighel, Lebedev Physical Institute, Leninsky Prospect 53, 117924 Moscow, U.S.S.R.
31. D. D. Ryutov, Institute of Nuclear Physics, Siberian Branch of the Academy of Sciences of the U.S.S.R., Sovetskaya St. 5, 630090 Novosibirsk, U.S.S.R.
32. V. T. Tolok, Kharkov Physical-Technical Institute, Academical St. 1, 310108 Kharkov, U.S.S.R.
33. R. Varma, Physical Research Laboratory, Navrangpura, Ahmedabad, India
34. Bibliothek, Max-Planck Institut fur Plasmaphysik, D-8046 Garching bei Munchen, Federal Republic of Germany

35. Bibliothek, Institut fur Plasmaphysik, KFA, Postfach 1913, D-5170 Julich, Federal Republic of Germany
36. Bibliotheque, Centre de Recherches en Physique des Plasmas, 21 Avenue des Bains, 1007 Lausanne, Switzerland
37. Bibliotheque, Service du Confinement des Plasmas, CEA, B.P. 6, 92 Fontenay-aux-Roses (Seine), France
38. Documentation S.I.G.N., Departement de la Physique du Plasma et de la Fusion Controlee, Centre d'Etudes Nucleaires, B.P. No. 85, Centre du Tri, 38041 Cedex, Grenoble, France
39. Library, Culham Laboratory, UKAEA, Abingdon, Oxfordshire, OX14 3DB, England
40. Library, FOM Instituut voor Plasma-Fysica, Rijnhuizen, Jutphaas, The Netherlands
41. Library, Institute of Physics, Academia Sinica, Beijing, Peoples Republic of China
42. Library, Institute of Plasma Physics, Nagoya University, Nagoya 64, Japan
43. Library, International Centre for Theoretical Physics, Trieste, Italy
44. Library, Laboratorio Gas Ionizzati, Frascati, Italy
45. Library, Plasma Physics Laboratory, Kyoto University, Gokasho Uji, Kyoto, Japan
46. Plasma Research Laboratory, Australian National University, P.O. Box 4, Canberra, A.C.T. 2000, Australia
47. Thermonuclear Library, Japan Atomic Energy Research Institute, Tokai, Naka, Ibaraki, Japan
48. J. F. Clarke, Associate Director for Fusion Energy, Office of Fusion Energy, Office of Energy Research, Mail Stop G-256, U.S. Department of Energy, Washington, DC 20545
49. D. B. Nelson, Acting Director, Division of Applied Plasma Physics, Office of Fusion Energy, Office of Energy Research, Mail Stop G-256, U.S. Department of Energy, Washington, DC 20545
50. M. N. Rosenbluth, RLM 11.218, Institute for Fusion Studies, University of Texas, Austin, TX 78712
51. W. Sadowski, Fusion Theory and Computer Services Branch, Office of Fusion Energy, Office of Energy Research, Mail Stop G-256, U.S. Department of Energy, Washington, DC 20545
52. A. Opdenaker, Reactor Systems and Applications Branch, Office of Fusion Energy, Office of Energy Research, Mail Stop G-256, U.S. Department of Energy, Washington, DC 20545
53. P. M. Stone, Reactor Systems and Applications Branch, Office of Fusion Energy, Office of Energy Research, Mail Stop G-256, U.S. Department of Energy, Washington, DC 20545
54. W. R. Ellis, Mirror Systems Branch, Office of Fusion Energy, Office of Energy Research, Mail Stop G-256, U.S. Department of Energy, Washington, DC 20545
55. J. M. Turner, Mirror Systems Branch, Office of Fusion Energy, Office of Energy Research, Mail Stop G-256, U.S. Department of Energy, Washington, DC 20545
56. J. Cowles, Mirror Systems Branch, Office of Fusion Energy, Office of Energy Research, Mail Stop G-256, U.S. Department of Energy, Washington, DC 20545

57. Theory Department Read File, c/o D. W. Ross, Institute for Fusion Studies, University of Texas at Austin, Austin, TX 78712
58. Theory Department Read File, c/o R. C. Davison, Director, Plasma Fusion Center, 167 Albany Street, Cambridge, MA 02139
59. Theory Department Read File, c/o F. W. Perkins, Princeton Plasma Physics Laboratory, P.O. Box 451, Princeton, NJ 08544
60. Theory Department Read File, c/o L. Kovrizhnykh, Levedev Institute of Physics, Academy of Sciences, 53 Leninsky Prospect, Moscow, U.S.S.R. V312
61. Theory Department Read File, c/o B. B. Kadomtsev, I. V. Kurchatov Institute of Atomic Energy, P.O. Box 3402, Moscow, U.S.S.R. 123182
62. Theory Department Read File, c/o T. Kamimura, Institute of Plasma Physics, Nagoya University, Nagoya, Japan
63. Theory Department Read File, c/o C. Mercier, Euratom-CEA, Service de Recherches sur la Fusion Controlee, Fontenay-aux-Roses (Seine), France
64. Theory Department Read File, c/o T. E. Stringer, JET Joint Undertaking, Culham Laboratory, Abingdon, Oxfordshire, OX14 3DB, England
65. Theory Department Read File, c/o K. Roberts, Culham Laboratory, Abingdon, Oxon, OX14 3DB, England
66. Theory Department Read File, c/o D. Biskamp, Max-Planck-Institut fur Plasmaphysik, D-8046 Garching bei Munchen, Federal Republic of Germany
67. Theory Department Read File, c/o T. Takeda, Japan Atomic Energy Research Institute, Tokai, Naka, Ibaraki, Japan
68. Theory Department Read File, c/o C. S. Liu, GA Technologies, Inc., P.O. Box 81608, San Diego, CA 92138
69. Theory Department Read File, c/o L. D. Pearlstein, Lawrence Livermore National Laboratory, P.O. Box 808, Livermore, CA 94550
70. Theory Department Read File, c/o R. Gerwin, CTR Division, MS 640, Los Alamos National Laboratory, P.O. Box 1663, Los Alamos, NM 87545
71. R. E. Mickens, Atlanta University, Department of Physics, Atlanta, GA 30314
72. R. A. Jong, L-637, Lawrence Livermore National Laboratory, P.O. Box 5511, Livermore, CA 94550
73. J. Gaffey, IPSI, University of Maryland, College Park, MD 20742
74. M. Iksea, R1/1070, TRW Defense and Space Systems, One Space Park, Redondo Beach, CA 90278
75. B. Fried, University of California at Los Angeles, Los Angeles, CA 90024
76. K. Matsuda, GA Technologies, Inc., P.O. Box 81068, San Diego, CA 92138
77. C. Grebogi, Plasma Physics Laboratory, University of Maryland, College Park, MD 20742
78. A. Ram, Room 38-256, Massachusetts Institute of Technology, Cambridge, MA 02139
79. V. S. Chen, GA Technologies, Inc., P.O. Box 81608, San Diego, CA 92138
80. B. Lembege, Physics Department, University of California at Los Angeles, Los Angeles, CA 90024
81. G. Rembel, Lawrence Livermore National Laboratory, P.O. Box 5511, Livermore, CA 94550

82. C. F. F. Kerney, Princeton Plasma Physics Laboratory, P.O. Box 451, Princeton, NJ 08544
83. J. Y. Hsu, GA Technologies, Inc., P.O. Box 81608, San Diego, CA 90024
84. G. R. Smith, Lawrence Livermore National Laboratory, P.O. Box 5511, Livermore, CA 94550
85-190. Given distribution as shown in TID-4500 Magnetic Fusion Energy (Category Distribution UC-20)

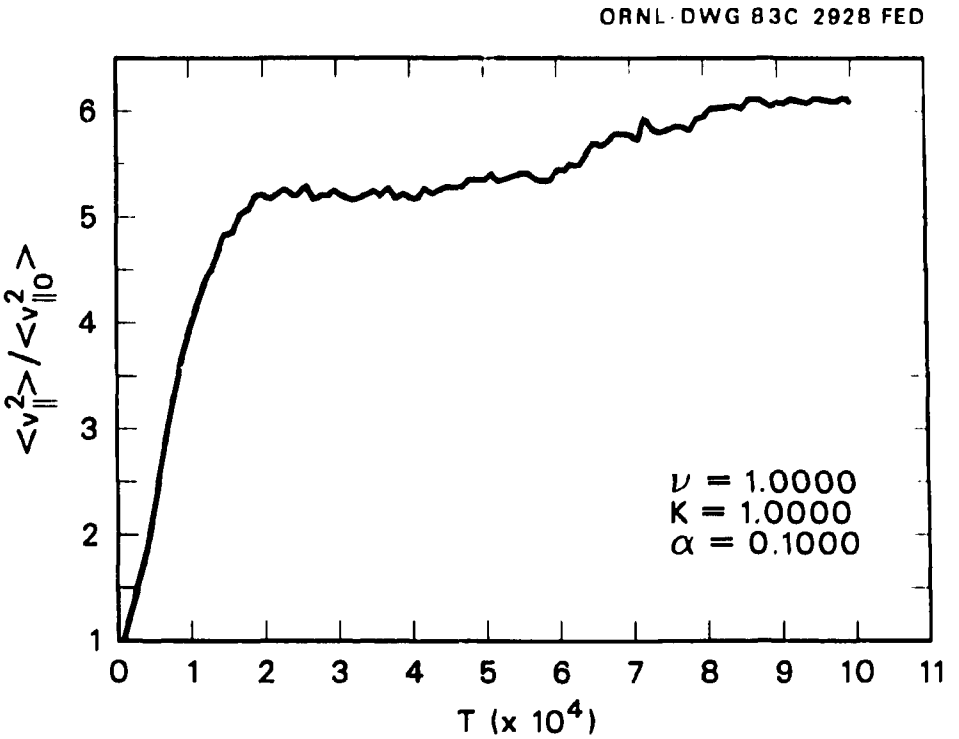
ORNL-DWG 83C 2928 FED
$\langle v_{\parallel}^2 \rangle / \langle v_{\parallel 0}^2 \rangle$
T (x 10^4)
ν = 1.0000
K = 1.0000
α = 0.1000

FIG. 9.